Defense Technical Information Center Compilation Part Notice

ADP014079

TITLE: Advances in Structural Integrity Analysis Methods for Aging Metallic Airframe Structures with Local Damage

This paper is part of the following report:

TITLE: Ageing Mechanisms and Control. Specialists' Meeting on Life Management Techniques for Ageing Air Vehicles [Les mecanismes vieillissants et le controle] [Reunions des specialistes des techniques de gestion du cycle de vie pour vehicules aeriens vieillissants]

To order the complete compilation report, use: ADA415672

The following component part numbers comprise the compilation report:
ADP014058 thru ADP014091

Advances in Structural Integrity Analysis Methods for Aging Metallic Airframe Structures with Local Damage

James H. Starnes*, Jr., James C. Newman, Jr., Charles E. Harris,
Robert S. Piascik, Richard D. Young and Cheryl A. Rose
*NASA Langley Research Center
Mail Stop 190
Hampton, VA 23681-2199, USA

ABSTRACT

Analysis methodologies for predicting fatigue-crack growth from rivet holes in panels subjected to cyclic loads and for predicting the residual strength of aluminum fuselage structures with cracks and subjected to combined internal pressure and mechanical loads are described. The fatigue-crack growth analysis methodology is based on small-crack theory and a plasticity induced crack-closure model, and the effect of a corrosive environment on crack-growth rate is included. The residual strength analysis methodology is based on the critical crack-tip-opening-angle fracture criterion that characterizes the fracture behavior of a material of interest, and a geometric and material nonlinear finite element shell analysis code that performs the structural analysis of the fuselage structure of interest. The methodologies have been verified experimentally for structures ranging from laboratory coupons to full-scale structural components. Analytical and experimental results based on these methodologies are described and compared for laboratory coupons and flat panels, small-scale pressurized shells, and full-scale curved stiffened panels. The residual strength analysis methodology is sufficiently general to include the effects of multiple-site damage on structural behavior.

KEYWORDS: fatigue-crack growth, critical crack-tip-opening-angle fracture criterion, nonlinear structural analysis, residual strength analysis, test-analysis correlation.

INTRODUCTION

Modern design philosophies for transport aircraft fuselage structures require that these structures retain adequate structural integrity when discrete source damage or fatigue cracks are present. As economic factors encourage the use of commercial and military transport aircraft beyond their original design requirements, it is important to develop methods that accurately predict the fatigue life and the residual strength of fuselage structures with cracks. During the past decade, research conducted at NASA Langley Research Center has resulted in a fatigue-crack growth analysis methodology for aircraft structures subjected to cyclic loads, and a residual strength analysis methodology for aluminum fuselage structures with cracks and subjected to combined internal pressure and mechanical loads. The fatigue-crack growth analysis methodology is based on small-crack theory and a plasticity induced crack-closure model (Ref. 1). The residual strength analysis methodology is based on elastic-plastic fracture mechanics and nonlinear structural analyses (Ref. 2), and is general enough to include the effects of multiple-site damage. This methodology includes a critical crack-tip-opening-angle (CTOA) fracture criterion (e.g., Refs. 3 and 4), and the STAGS (STructural Analysis of General Shells) nonlinear finite element shell analysis code (Ref. 5). The critical CTOA criterion assumes that stable crack growth will occur when the local crack opening angle reaches a critical value, and STAGS is used with the critical CTOA criterion to perform residual strength analyses for structures with geometric and material nonlinear characteristics.

Paper presented at the RTO AVT Specialists' Meeting on "Life Management Techniques for Ageing Air Vehicles", held in Manchester, United Kingdom, 8-11 October 2001, and published in RTO-MP-079(II).

The present paper describes the fatigue-crack growth analysis and the residual strength analysis methodologies developed at NASA Langley Research Center, and presents results from several studies (Refs. 6-11) that have applied these methodologies to test specimens ranging in complexity from small laboratory coupon specimens to full-scale 2024-T3 stiffened fuselage panels. The fracture parameters used to predict the residual strength behavior of the more complex test specimens were obtained from the small laboratory coupon specimens. Results are presented for unstiffened and stiffened flat panels, small-scale unstiffened shells, and full-scale curved stiffened fuselage panels.

FATIGUE CRACK GROWTH ANALYSIS METHODOLOGY

The fatigue life prediction methodology developed at NASA Langley Research Center is based on 'small-crack theory' and a plasticity induced crack-closure model. 'Small-crack theory' is the treatment of fatigue as a crack propagation process from a micro-defect (or crack) to failure. The propagation of small fatigue cracks from surface defects (5 μm to 10 μm) constitutes a large percentage (50% to 90%) of the total fatigue life of structural components. Thus, accurate prediction of small-crack growth rate is required for damage-tolerance-based life predictions. The fatigue life prediction methodology is described in Ref. 6 and summarized in this section. First, large-crack fatigue-crack growth rate data from testing small laboratory coupon specimens are used to develop the relationship between the effective stress-intensity factor range (ΔK_{eff}) and crack-growth rate for a constant-amplitude loading condition. The effective stress-intensity factor range (ΔK_{eff}) accounts for plasticity-induced crack closure, and is used to define the closure-free ΔK-rate relation. A constraint factor, α, which accounts for three-dimensional state-of-stress effects, is used as a fitting parameter to correlate crack-growth rate data with ΔK_{eff} for constant-amplitude loading conditions with different stress ratios. Then, the ΔK_{eff}-rate relationship or curve in the near-threshold regime is modified to fit measured small-crack growth-rate behavior and fatigue endurance limits. The resulting ΔK_{eff}-rate relationship is used as input to the life-prediction code FASTRAN-II (Ref. 1) to predict the total fatigue life of a structural component based on crack propagation from micro-structural features. A crack is assumed to initiate and grow from a micro-structural feature (e.g., inclusion particle, void, corrosion pit) on the first cycle (e.g., Ref. 12). The crack-closure model and ΔK_{eff}-rate curve are used to predict crack growth from the initial crack size to failure.

Prediction of Crack Growth and Fatigue Life of 4340 Steel

Comparisons between small- and large-crack results have been made for 4340 steel (Refs. 13 and 14). A baseline effective stress-intensity factor range versus crack-growth rate curve for the material was developed in Ref. 13, and this curve was used to predict small-crack growth rate behavior from extremely small initial crack sizes on the notched specimens in Ref. 14. In Ref. 14, large-crack results were obtained from middle-crack tension specimens, and small-crack data were obtained from single-edge-notch tension specimens. The plastic-replica method was used to measure the growth of small cracks. Examination of the initiation sites for 35 fatigue cracks gave information on the distribution of crack-initiation site dimensions. The most dominant crack-initiation site particle was a spherical (calcium-aluminate) particle. The mean defect was about 13-μm in radius. Over 80% of all defects were represented by upper and lower bounds for the defect sizes of 8- and 30-μm in radius.

A comparison of small- and large-crack data for 4340 steel is shown in Figure 1(a). The symbols represent small surface-crack data from the single-edge-notch tension specimens. The dashed-dot curve represents the large-crack data obtained from middle-crack tension specimens. The small cracks were measured in the thickness or a-direction and large cracks were measured in the width or c-direction. The small- and large-crack data agree quite well. The dashed curve is the ΔK_{eff}-rate curve from Ref. 13, determined from middle-crack tension specimen data. The constraint factor α is 2.5 for rates less than 5E-4 mm/cycle. The solid curves are the predicted results from FASTRAN (Ref. 1) with either

an initial semi-circular surface crack of 8- or 30-μm. All predictions start on the ΔK_{eff}-rate curve because the initial crack is assumed to be fully open on the first cycle. Because the effective stress-intensity factor curve is near to the large-crack curve, small-crack effects are weak. The predicted results for the largest defect size rapidly approach the large-crack behavior. The predicted results for the smallest defect size decrease very rapidly and then increase very rapidly to the large-crack curve. This behavior is due to the crack-closure transient and the shape of the ΔK_{eff}-rate curve at the lower rates.

The results from Ref. 14, shown in Fig. 1(a), were applied by Everett (Ref. 15) to predict the response of fatigue tests on 4340 steel (thickness B = 3.2 mm) using a specimen of width w = 12.7 mm and a single open hole with radius r = 3.2 mm. The material used in Ref. 15 had the same strength level as the material tested in Ref. 14, but the specimens were thinner and were taken from a different heat of material. However, it was assumed that the large-crack data and inclusion-particle sizes would be the same. A small-crack effective threshold, $(\Delta K_{eff})_{th}$, of 3.2 MPa$\sqrt{m}$ was used to predict the endurance limits or the applied stress level where the initial defect would not grow. Results of constant-amplitude fatigue tests with a stress ratio R = 0 are shown by the symbols in Figure 1(b) for open-hole specimens. The maximum stress in the spectrum is plotted versus the number of cycles to failure. Predictions of total fatigue life were made using the FASTRAN code (Ref. 1) by calculating the number of cycles necessary to grow a crack from 8- and 30-μm initial semi-circular surface cracks located at the center of the hole. Near the endurance limit, the analysis results bound the test data quite well, but predict slightly longer lives at the highest stress levels for the tests. The defect size had more influence on life in the endurance limit regime than for the higher stress levels.

The Effect of Corrosion on Fatigue Life

Constant-amplitude fatigue-crack growth experiments were conducted (Ref. 7) in laboratory air and deaerated 1% NaCl environments to determine the effects of a corrosive environment on the ΔK_{eff}-rate relationship for 2024-T3 aluminum alloy. Extended compact-tension or eccentrically loaded single-edge cracked-tension specimens were tested for different R ratios ranging from 0.05 to 0.80. Small surface and corner crack growth rates and stress intensity factors were calculated assuming uniform semicircular crack geometry. The results of these tests are shown in Fig. 2(a) and indicate that the NaCl environment can accelerate the crack-growth rate. The fatigue cracks initiated at a corrosion pit approximately 10 μm in depth located at the root of the blunt notch in the specimens. Following initiation, the crack propagated along a transgranular semicircular shaped crack path.

A series of tests were conducted by Furuta, et al. (Ref. 16) to study the fatigue behavior of 2024-T3 (Alclad) countersink-riveted lap-joint panels exposed to a room-temperature laboratory air environment and a 3.5% NaCl corrosive salt-water environment. A typical test of a panel with two rows of rivets was conducted at a constant-amplitude loading condition with R = 0.125 and maximum stress S_{max} = 96 MPa to simulate fuselage skin stress conditions. A fastener interference level was not used in any calculations, and fastener bending effects were not included. The two-rivet row had a 50% rivet and by-pass stress. The results shown in Fig. 2(b) indicate that the fatigue life of the panels exposed to salt water (square symbol) is reduced by a factor of about 1/2 or 1/3 compared to the fatigue life in ambient laboratory air (circle symbol). The FASTRAN (Ref. 1) predictions for salt water and laboratory air environments are in excellent agreement with the experimental results. The fracture mechanics based calculations assumed a corner crack in a neat-fit riveted-loaded straight-shank hole (rivet fit-up and interference fit stresses are assumed small). The 6 μm radius equivalent initial flaw size used for each FASTRAN prediction is consistent with laboratory observations; 6 μm radius constituent particles and corrosion pits are observed at small crack initiation sites in fatigue test coupons exposed to laboratory air and salt water, respectively (Ref. 7). The predicted fatigue lives shown in Fig. 2(b) agree well with the test results.

RESIDUAL STRENGTH ANALYSIS METHODOLOGY

The residual strength analysis methodology developed at NASA Langley Research Center is based on the critical crack-tip-opening-angle (CTOA) fracture criterion (e.g., Refs. 3 and 4) and the STAGS nonlinear shell analysis code (Ref. 5). This analysis methodology accounts for both material and geometric nonlinear behavioral characteristics of the materials and structures of interest. The following sections describe the CTOA fracture criterion, and the geometric and material nonlinear finite element shell analysis code STAGS used in the residual strength analysis methodology.

CTOA Fracture Criterion and Plane-Strain-Core Height

The critical CTOA fracture criterion is supported by experimental measurements of the critical angle during stable growth and has been shown to be well suited for modeling stable crack growth in ductile materials and for predicting the onset of unstable crack growth in fracture analyses conducted using elastic-plastic finite element methods (e.g., Refs. 3 and 4). The CTOA is defined as the angle made by the upper crack surface, the crack tip, and the lower crack surface, evaluated at a fixed distance from the moving crack tip, as illustrated in Fig. 3. A fixed distance of 1 mm is used in the present paper to evaluate the critical CTOA value (e.g., Ref. 10). The CTOA criterion assumes that crack extension will occur when the CTOA reaches a critical value, $CTOA_{cr}$, and that the $CTOA_{cr}$ will remain constant as the crack extends. The critical CTOA value can be obtained experimentally using a photographic technique (Ref. 4), but significant scatter is usually present in the measurements. A better method of determining the critical CTOA value is to simulate the fracture behavior of a laboratory specimen with a three-dimensional elastic-plastic finite element analysis and determine the angle that best describes the experimentally observed fracture behavior.

An example demonstrating the use of a three-dimensional, elastic-plastic finite element analysis to determine the critical CTOA for three different thicknesses of 2024-T3 aluminum alloy, is shown in Fig. 4, where the critical value of CTOA for each thickness is represented by the symbol Ψ_c. Results of compact tension (C(T)) laboratory tests are shown in Fig. 4 for 2024-T3 aluminum-alloy sheets with the cracks parallel to the sheet rolling direction. The compact-tension test specimens are 152-mm wide with an initial crack length a = 61 mm. Data for three difference sheet thicknesses are shown on the figure. Analytical results from the geometrically linear elastic-plastic three-dimensional finite element code ZIP3D (Ref. 17) are also shown on the figures, and the critical CTOA values represent the best fit with the test data.

A three-dimensional finite element analysis code, such as ZIP3D, requires only the critical CTOA to predict the fracture behavior of thin ductile materials, since three-dimensional constraint effects that develop at the local crack tip (Ref. 18) are explicitly accounted for in the model. In a finite element shell analysis code, which typically uses two-dimensional plane-stress elements, a modeling approximation is required to simulate the actual state of stress near the crack tip. The modeling approximation used in the present methodology is to introduce a thin strip of plane-strain elements in a region on each side of the crack line. The width of the plane-strain region on each side of the crack line is commonly referred to as the plane-strain-core height, h_c, and is approximately equal to the thickness of the specimen. This strip of plane-strain elements has plane-strain conditions, while the remainder of the model has plane-stress conditions, as illustrated in Figure 5. The plane-strain-core height h_c is determined from analyses using the two-dimensional ZIP2D code (Ref.19), and the critical angle determined from the ZIP3D analysis is used to determine the value of h_c that makes the ZIP2D analysis results consistent with the ZIP3D results, as shown in Fig. 5.

To confirm that fracture parameters determined in the manner described above could be applied in a STAGS analysis, geometrically nonlinear elastic-plastic analyses were conducted to predict the fracture response in the T-L orientation of 1.6-mm-thick,

2024-T3 compact-tension (C(T)), and middle-crack tension (M(T)) panels, with and without buckling constraints. The critical CTOA used in the analyses was equal to 5.0°, and the plane-strain-core height, h_c = 1 mm. The experimental and predicted crack extension results for the C(T) and M(T) panels are shown in Fig. 6 as a function of the applied load. These results verify the selection of $CTOA_{cr}$ = 5.0° and h_c = 1mm for the material and indicate that the analyses with STAGS accurately predict the reduction in strength of the panels caused by the geometrically nonlinear effect of panel buckling.

Nonlinear Structural Analysis Code

The STAGS (STructural Analysis of General Shells) nonlinear shell analysis code (Ref. 5) is used in the residual strength analysis methodology to predict the response and residual strength of unstiffened aluminum shells and stiffened aluminum fuselage panels with longitudinal cracks. STAGS is a finite element code for analyzing general shells and includes the effects of geometric and material nonlinearities in the analysis. STAGS can perform crack-propagation analyses, and can represent the effects of crack growth on nonlinear shell response. A nodal release method and a load relaxation technique are used to extend a crack while the shell is in a nonlinear equilibrium state. The changes in the stiffness matrix and the internal load distribution that occur during crack growth are accounted for in the analysis, and the nonlinear coupling between internal forces and in- and out-of-plane displacement gradients that occurs in a shell are properly represented.

Finite element models are constructed using a collection of two-node beam elements, two-node fastener elements, and four-node plate elements. Each node of the models has six degrees of freedom. Structural components including skins, stringers, frames, tear straps, and stringer clips are modeled by plate elements to represent accurately the cross sectional shapes of all components. Riveted connections between structural components are modeled using beam elements, or fastener elements in the region close to a crack, where fastener flexibility is thought to affect load transfer. The fastener elements represent the offsets of the joined components with rigid links that are connected by spring elements with six degrees of freedom. The spring elements can model elastic-plastic behavior, and fastener breakage if a prescribed fastener strength is exceeded. An example of fastener modeling details is given in Ref. 20. For conditions where deformation of the model would cause interpenetration of elements, the general contact capability in STAGS is invoked to prevent such element interpenetration from occurring. To simulate the experimental conditions for the specimens considered in the present paper, the finite element models include the load introduction hardware and replicate the loading conditions as applied in the experiments.

PANEL AND SHELL TEST AND ANALYSIS RESULTS

The residual strength analysis methodology described in the present paper has been experimentally verified for structures ranging in size from laboratory coupons to full-scale structural components. Results for small-scale pressurized shells, flat stiffened panels, and curved stiffened panels are presented in this section. Analysis results were obtained using values of $CTOA_{cr}$ and h_c that were determined for each material, sheet thickness, and crack orientation by correlating elastic-plastic finite element analyses and experimental results for small laboratory specimens.

Pressurized Cylindrical Shell Tests

Cylindrical shells were fabricated from 1-mm-thick 2024-T3 aluminum-alloy sheet, with the rolling direction orientated circumferentially. The shells were 99-cm long, 45.7 cm in diameter, and had a 3.8-cm-wide double lap splice with 1-mm-thick splice plates and a single row of rivets on each side of the splice. Each shell had a longitudinal crack that was simulated by a 0.025-mm-wide saw cut at the specimen mid-length, diametrically opposite to the lap-splice. Specimens with initial crack lengths of 50.8,

76.2, and 101.6 mm were loaded by internal pressure until failure occurred (Ref. 8). The crack length extension was recorded using crack wire gages.

The experimental measurements and the STAGS finite element predictions for the pressurized cylindrical shells are shown in Figure 7. Analysis predictions were made using $CTOA_{cr} = 5.6°$, and $h_c = 1$ mm. For all crack lengths, the analyses predicted the maximum pressure to within 4% of the measured values, but tended to overpredict the pressure required to initiate crack growth. The use of saw cuts would generally cause the analysis to underpredict the pressure required to initiate the crack growth, since a saw cut would require higher loads to initiate crack growth than a sharp fatigue crack. One possible explanation for the overprediction of the crack growth initiation pressure could be that the intense crack-tip deformations might have caused the crack wire gages to register crack growth before the growth actually occurred.

Flat Stiffened Panel Tests

Fracture tests were conducted on 1016-mm-wide, 1.6-mm-thick, 2024-T3 aluminum alloy, flat, stiffened panels (Ref. 21). The stiffeners were made from 7075-T3 aluminum alloy and riveted to the specimens. The stiffeners were 40.6-mm wide and placed on both sides of the specimen, as shown in Figure 8. The crack configuration consisted of a single 203-mm-long center crack with an array of twelve 4.7-mm-diameter holes on either side of the of the center crack. Specimens with and without MSD were tested. The MSD crack length was 1.27 mm from the edge of the hole. The specimens were tested without guide plates to allow out-of-plane displacements.

The experimental and analytical results for the stiffened panels with a single center crack and without and with MSD are shown in Figures 9(a) and 9(b), respectively. Predictions of the fracture behavior were conducted with STAGS using a critical CTOA value of 5.4°, and a plane-strain-core height of 2 mm. The results indicate that the analysis methodology represents the behavior of these specimens very well.

Curved Stiffened Panel Tests

Three stringer- and frame-stiffened aluminum fuselage panels with longitudinal cracks were tested and analyzed. These curved stiffened panels are referred to as Panels ASIP1, ASIP2, and ASIP3 in the present paper and are shown in Figure 10 prior to testing. The panels all had 3.09-m radii and initial crack lengths of 254 mm. Panels ASIP1 (Fig. 10(a)) and ASIP3 (Fig. 10(b)) had the initial crack located at the panel centerline, and panel ASIP2 (Fig. 10(c)) had the initial crack along a row of fasteners in a lap splice at the second stiffener. Panel ASIP2 also had MSD cracks along the fastener holes near the lead crack as shown in Figure 10(d). Panels ASIP1 and ASIP2 were 1.83-m long and panel ASIP3 was 3.5-m long. Additional details of the panels are given in Refs. 9 and 11. Panels ASIP1 and ASIP2 were tested in a pressure-box test machine and were subjected to combined internal pressure and mechanical hoop and axial tension loads. Panel ASIP3 was tested in the COLTS combined loads test facility located at NASA Langley Research Center. The panel was attached to a D-box test fixture, and subjected to internal pressure, axial compression and torsion loads. Details of the COLTS test facility and D-box test fixture for ASIP3, and the test and analysis results for ASIP3 are given in Ref. 11.

The test results for panel ASIP1 indicate that the panel arrested the propagating crack at the tear straps. As the internal pressure was increased, each end of the skin crack extended in the longitudinal direction until it intercepted an adjacent tear strap. The crack growth behavior was symmetric with respect to the central frame. The experimental and predicted crack extension results are compared in Fig. 11 as a function of pressure. Predictions of the fracture behavior were conducted with the STAGS analysis code using $CTOA_{cr} = 5.0°$, and $h_c = 1$ mm. These results indicate good agreement in the pressure corresponding to crack extension values up to 25.4 mm, but a discrepancy in the predicted and observed responses occurs for crack extension greater than 25.4 mm. In the experiment, after 25.4 mm of crack extension, very small increases in pressure cause

significant amounts of crack extension, while the analysis indicates that larger increases in pressure are required for additional crack extension. The values of the pressure for the test and the analysis differ by only 1% for 25.4 mm. of crack extension, but differ by 10% for 50.8 mm of crack extension.

The test results for panel ASIP2 indicate that the panel failed as a result of MSD crack link up. At a certain pressure magnitude, the lead crack suddenly extended on each end of the crack, and linked up with the series of MSD cracks ahead of the lead crack. The crack extended in the longitudinal direction in a fast fracture mode, and extended over the entire panel length in an instant. The crack growth behavior was symmetric with respect to the central frame. A typical solution with crack growth in the lead crack and the MSD cracks is shown in Fig. 12. The contour plot of the hoop stress in the region around the crack tip region, shown in Fig. 12(a), indicates the high stress regions near the crack tips of the lead crack and the MSD cracks. A contour plot of the plastic strains in the hoop direction is shown in Fig. 12(b) which indicates that there are regions of plastic deformation emanating from the lead crack and from the MSD crack tips, and that for the solution shown, the plastic zones from the lead crack and the first MSD crack have coalesced. The deformed shape shown in these plots indicates that the deformation on the side of the crack attached to the stiffener is much smaller than the deformation on the other side of the crack, demonstrating that the crack is not tearing due to a symmetric loading condition. The asymmetric loading could promote curvilinear crack growth, but it is assumed in the analysis that interaction between the lead crack and the MSD cracks will cause self-similar crack growth. The opening of the MSD cracks is also evident in the deformed shapes. The crack extension response from the analysis and the experiment are compared in Fig. 13 as a function of pressure. Predictions of the fracture behavior were obtained using $CTOA_{cr} = 5.0°$, and $h_c = 1$ mm. The breaks in the solid curve indicate locations where the lead crack linked up with the MSD cracks to create a discontinuity in the length of the lead crack. Thus, the analysis predicts fast fracture and link-up at a pressure that is 11% greater than what was observed in the experiment. For comparison purposes, the predicted response of panel ASIP1 is also included in Fig. 13. The difference in the predicted stability of the tearing response of these two panels is caused by the interaction of the lead crack and the MSD cracks in panel ASIP2.

CONCLUDING REMARKS

A plasticity induced crack-closure model has been used to correlate large-crack growth-rate data for a constant-amplitude loading condition in ambient and corrosive environments. Comparisons made between measured and predicted small-crack growth rates indicate that the closure model predicts the trends of the test results. Using the closure model and some microstructural features, such as inclusion-particle sizes, a fatigue-life prediction method has been demonstrated for materials of interest. Predicted fatigue lives for notched specimens compare well with test data under constant-amplitude and spectrum loading. It is likely that a panel with a large number of fastener holes and other areas of stress concentration may have a critical size inclusion particle located at one of these sites. Thus, using the largest material defect for a material of interest, such as the 30-μm defect, would produce a somewhat conservative but reliable life prediction. If there are manufacturing defects larger than the material defects, they would control the fatigue lives of components subjected to cyclic loading conditions.

A residual strength analysis methodology for aircraft aluminum fuselage structures with cracks and subjected to combined internal pressure and mechanical loads has been used to predict the crack propagation characteristics of structures ranging from laboratory coupons to full-scale structural components. The methodology is based on the critical crack-tip-opening-angle fracture criterion that characterizes the fracture behavior of a material of interest, and a geometric and material nonlinear finite element shell analysis code that performs the structural analysis of the fuselage structure of interest. The methodology is sufficiently general to include the effects of multiple-site damage on

structural behavior. Analytical results based on this methodology are compared with experimental results for aluminum-alloy laboratory coupons and flat panels, small-scale pressurized shells, and full-scale curved stiffened panels. The analytical and experimental results compare well.

The results of residual strength analyses indicate that elastic-plastic effects in a thin sheet can be effectively represented by a critical crack-tip-opening-angle fracture criterion. The results also indicate that geometric and material nonlinear structural analyses can accurately represent the changes in internal load distributions, local stress and displacement gradients, and crack growth behavior in stiffened fuselage shells with long cracks and subjected to combined internal pressure and mechanical loads. In addition, nonlinear fracture analysis and structural analysis methods provide higher fidelity results than traditional linear-elastic engineering analysis approximations for structures with significant plastic yielding and nonlinear out-of-plane deformations associated with internal pressure loads.

REFERENCES

1. Newman, J. C., Jr., "FASTRAN-II - A Fatigue Crack Growth Structural Analysis Program," NASA TM 104159, 1992.
2. Harris, C. E., Newman, J. C., Jr., Piascik, R. S., and Starnes, J. H., Jr., "Analytical Methodology for predicting the Onset of Widespread Fatigue Damage in Fuselage Structure," *Journal of Aircraft,* Vol. 35, No. 2, 1998, pp. 307-317.
3. Newman, J.C., Jr., "An Elastic-Plastic Finite Element Analysis of Crack Initiation, Stable Crack Growth, and Instability," ASTM STP 833, 1984, pp. 93-117.
4. Dawicke, D. S., Sutton, M. A., Newman, J. C., Jr., and Bigelow, C. A., "Measurement and Analysis of Critical CTOA for an Aluminum Alloy Sheet," NASA TM-109024, September 1993.
5. Rankin, C. C., Brogan, F. A., Loden, W. A., and Cabiness, H. D., "STAGS User Manual, Version 3.0," Lockheed Martin Missiles and Space Co., Inc., Advanced Technology Center, Report LMMS P032594, June 1998.
6. Newman, J. C., Jr., "Advances in Fatigue and Fracture Mechanics Analyses for Metallic Aircraft Structures,"*Structural Integrity for the Next Millennium, Vol. 1*, Proceedings of the 20th Symposium of the International Committee on Aeronautical Fatigue, J. L. Rudd and R. M. Bader, eds., Bellingham, WA, July 14-16, 1999, pp. 3-40.
7. Piascik, R. S., and Willard, S. A., "The Growth of Small Corrosion Fatigue Cracks in Alloy 2024," *Fatigue and Fracture of Engineering Materials and Structures*, Vol. 17, No. 11, 1994, pp. 1247-1259.
8. Starnes, J. H., Jr., and Rose, C. A., "Stable Tearing and Buckling Response of Unstiffened Aluminum Shells with Long Cracks," Proceedings of the Second Joint NASA/FAA/DOD Conference on Aging Aircraft, Williamsburg, VA, August 31-September 3, 1998. NASA/CP-1999-208982/Part 1, January 1999, pp. 610-626.
9. Young, R. D., Rouse, M., Ambur, D. R., and Starnes, J. H., Jr., "Residual Strength Pressure Tests and Nonlinear Analyses of Stringer- and Frame-Stiffened Aluminum Fuselage Panels with Longitudinal Cracks," Proceedings of the Second Joint NASA/FAA/DOD Conference on Aging Aircraft, Williamsburg, VA, August 31-September 3, 1998. NASA/CP-1999-208982/Part 1, January 1999, pp. 408-426.

10. Dawicke, D. S., Newman, J. C., Jr., Starnes, J. H., Jr., Rose, C. A.; Young, R. D., and Seshadri, B. R., "Residual Strength Analysis Methodology: Laboratory Coupons to Structural Components," Proceedings of the Third Joint FAA/DOD/NASA Conference on Aging Aircraft, Albuquerque, NM, September 20-23, 1999.

11. Ambur, D. R., Rouse, M., Young, R. D., and Perez-Ramos, C., "Evaluation of an Aluminum Panel with Discrete-Source Damage and Subjected to Combined Loading Conditions," Proceedings or the 40th AIAA/ASME/ASCE/AHS/ASC Structures, Structural Dynamics, and Materials Conference, St. Louis, MO, April 12-15, 1999. AIAA Paper AIAA-99-1439, 1999.

12. Newman, J. C., Jr., and Edwards, P. R., "Short-Crack Growth Behaviour in an Aluminum Alloy - an AGARD Cooperative Test Programme," AGARD R-732, 1988.

13. Newman, J. C., Jr., Swain, M. H., and Phillips, E. P., "An Assessment of the Small Crack Effect for 2024-T3 Aluminum Alloy," *Small Fatigue Cracks*, R. O. Ritchie and J. Lankford, eds., 1986, pp. 427-452.

14. Swain, M. H., Everett, R. A., Newman, J. C., Jr., and Phillips, E. P., "The Growth of Short Cracks in 4340 Steel and Aluminum-Lithium 2090," AGARD R-767, P. R. Edwards and J. C. Newman, Jr., eds., 1990, pp. 7.1-7.30.

15. Everett, R. A., Jr., "A Comparison of Fatigue Life Prediction Methodologies for Rotorcraft," NASA TM 102759, 1990.

16. Furuta, S., Terada, H., and Sashikuma, H., "Fatigue Strength of Fuselage Joint Structures under Ambient and Corrosive Environment," *Fatigue in New and Ageing Aircraft*, R. Cook and P. Poole, eds., EMAS, Ltd., 1997, pp. 231-249.

17. Shivakumar, K. N., and Newman, J. C., Jr., "ZIP3D - An Elastic-Plastic Finite-Element Analysis Program for Cracked Bodies," NASA TM-102753, 1990.

18. Dawicke, D. S., Newman, J.C., Jr., and Bigelow, C. A., "Three-Dimensional CTOA and Constraint Effects During Stable Tearing in a Thin-Sheet Material," In *Fracture Mechanics: 26th Volume*, ASTM STP 1256, 1995, pp. 223-242.

19. Newman, J. C., Jr., "Finite Element Analyses of Fatigue Crack Propagation -- Including the Effects of Crack Closure," Ph.D. Thesis, Virginia Polytechnic institute and State University, Blacksburg, VA, May 1974.

20. Young, R. D., Rose, C. A., Dávila, C. G., Starnes, J. H., Jr., and Rankin, C. C., "Crack Growth and Residual Strength Characteristics of Selected Flat Stiffened Aluminum Panels," Proceedings of the First Joint DOD/FAA/NASA Conference on Aging Aircraft, Ogden, UT, July, 1997.

21. Seshadri, B. R., Newman, J. C., Jr., Dawicke, D. S., and Young, R. D., "Fracture Analysis of the FAA/NASA Wide Stiffened Panels," Proceedings of the FAA-NASA Symposium on the Continued Airworthiness of Aircraft Structures," DOT/FAA/AR-92/2, 1997, pp. 513-524.

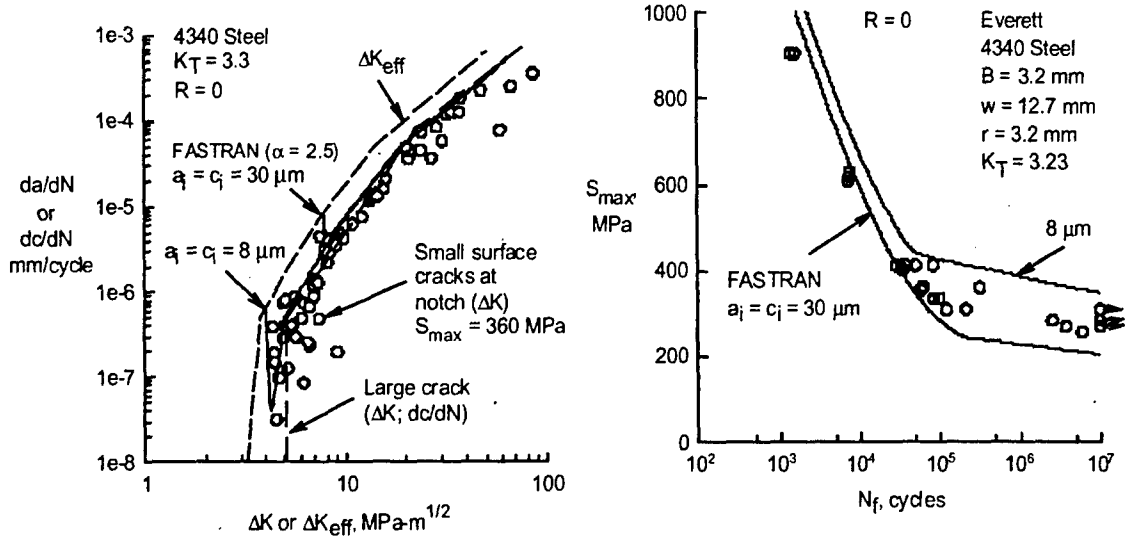

(a) Small corner crack growth rate at a notch.

(b) Fatigue lives.

Figure 1. Measured and predicted short crack growth rate and fatigue lives for 4340 steel.

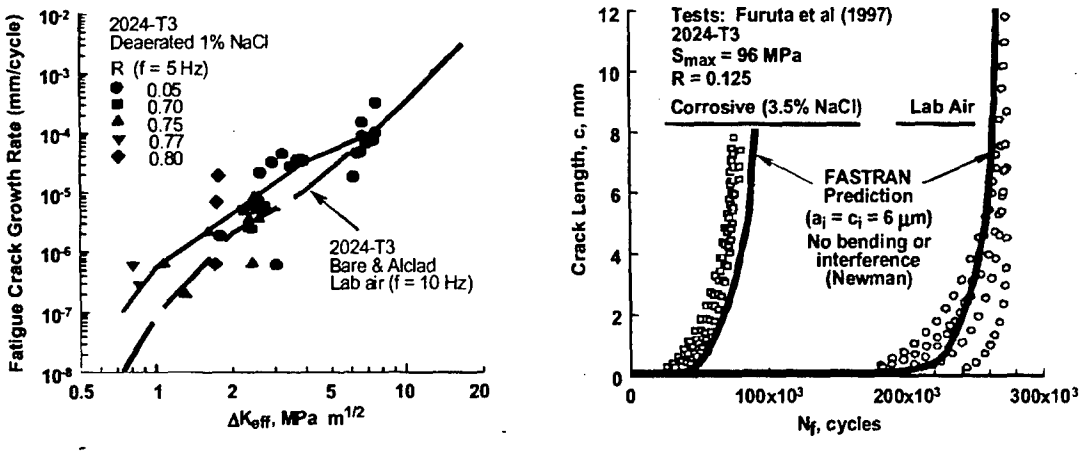

(a) Fatigue crack growth rate in air and salt solution.

(b) Lap joint fatigue crack growth.

Figure 2. The effect of corrosion on fatigue life.

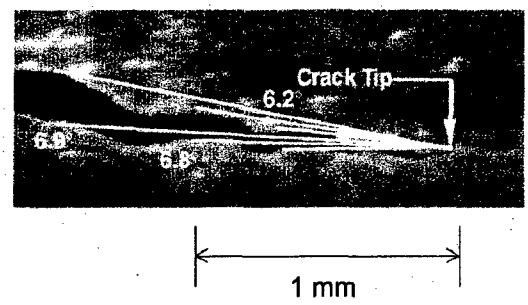

Figure 3. Critical crack-tip-opening-angle criterion.

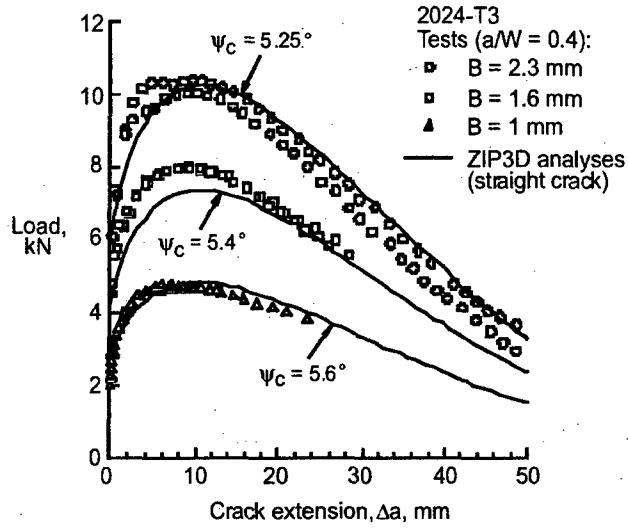

Figure 4. Experimental fracture measurements and ZIP3D finite element predictions for 152-mm-wide C(T) specimens of 2024-T3 aluminum alloy with an initial crack length of a/W = 0.4 and three specimen thicknesses.

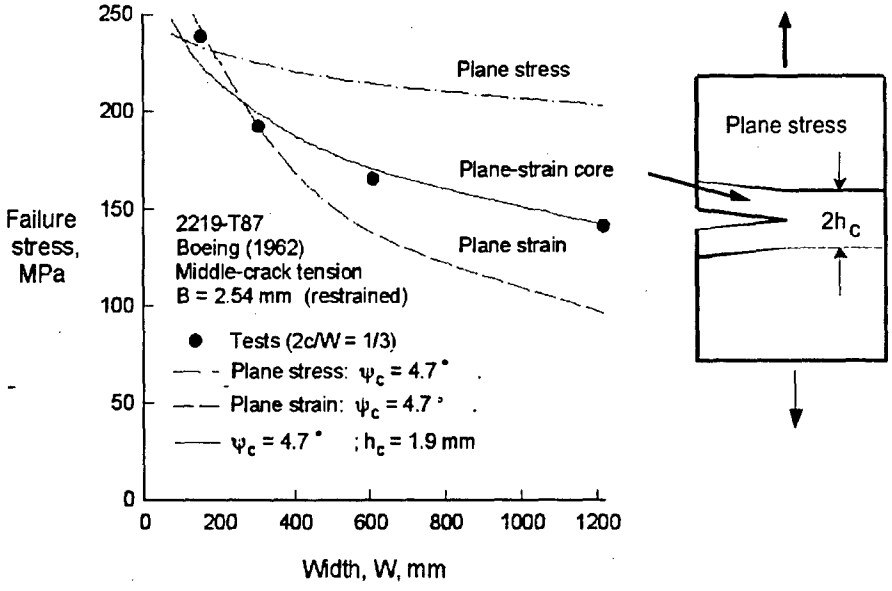

Figure 5. ZIP2D finite element predictions for C(T) specimens to determine plane-strain core height, h_c.

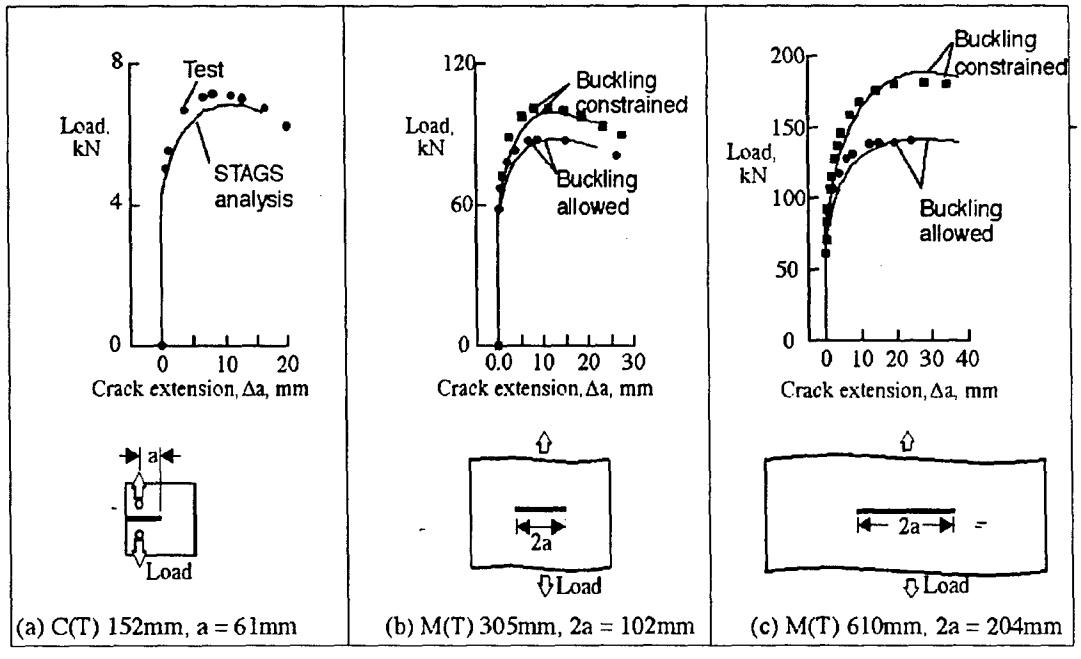

Figure 6. Load versus crack extension results from C(T) and M(T) tests, and nonlinear STAGS analyses with $CTOA_{cr} = 5.0°$ and $h_c = 1$ mm. Specimen widths w = 152, 305, and 610mm, respectively.

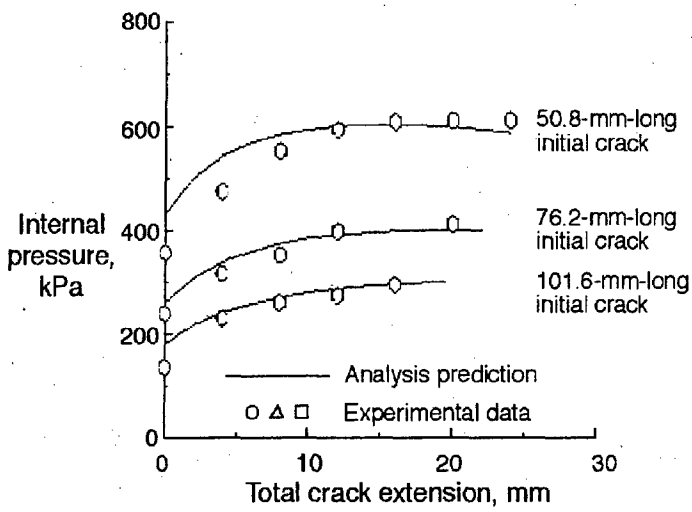

Figure 7. Comparison of analytical and experimental total crack extension results for 1-mm-thick internally pressurized unstiffened aluminum shells.

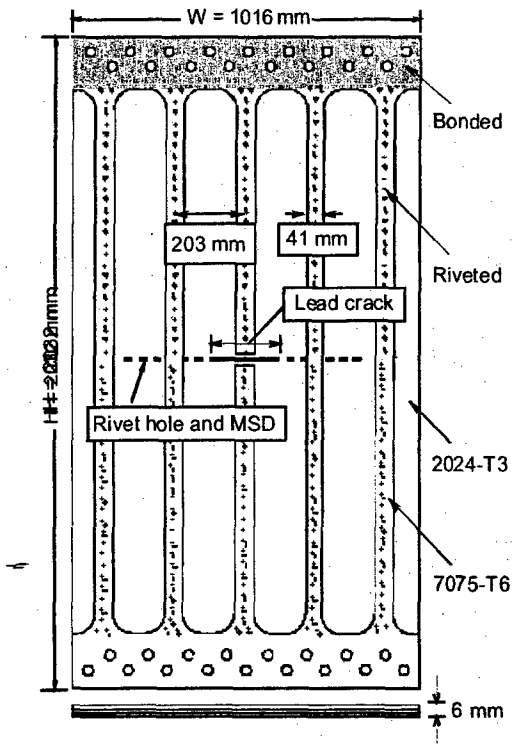

Figure 8. Wide stiffened flat aluminum panel and MSD configuration.

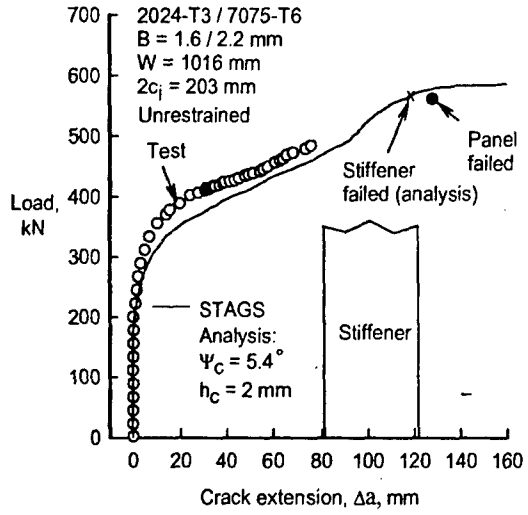

(a) Panel with a single crack.

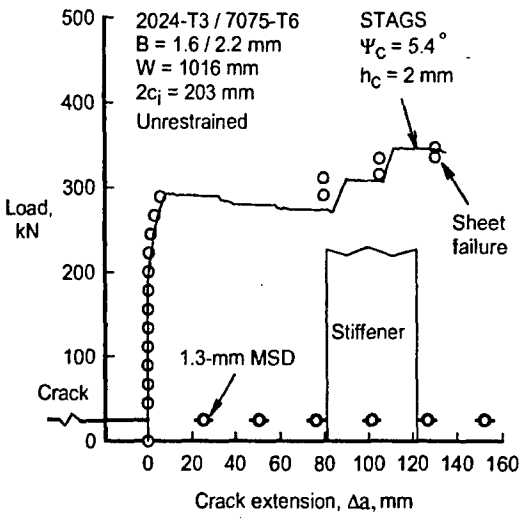

(b) Panel with MSD.

Figure 9. Experimental fracture measurements and STAGS finite element predictions for a 1016-mm-wide, 2024-T3 aluminum alloy unrestrained stiffened panel with a single crack without and with MSD cracks.

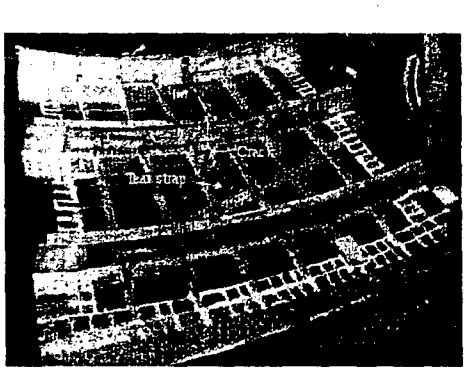

(a) Panel ASIP1 prior to testing.

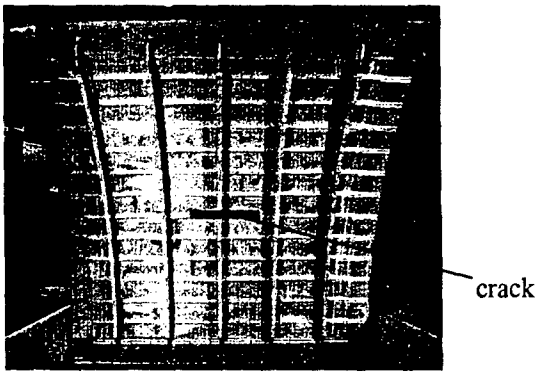

(b) Panel ASIP3 prior to testing.

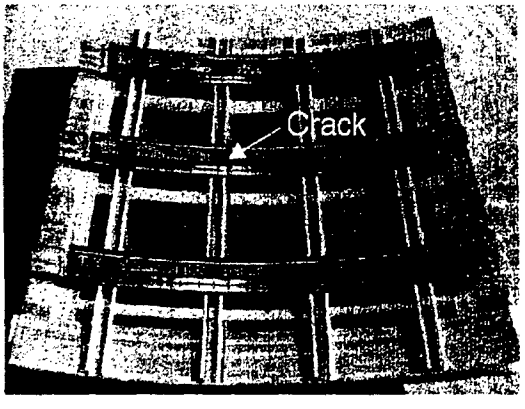

(c) Panel ASIP 2 prior to testing.

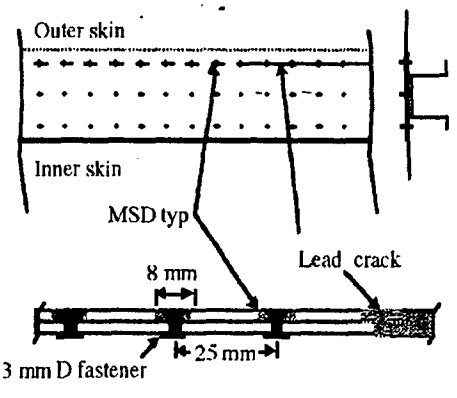

(d) Lap joint detail with lead crack and MSD cracks for panel ASIP2.

Figure 10. ASIP1, ASIP2, ASIP3 test panels.

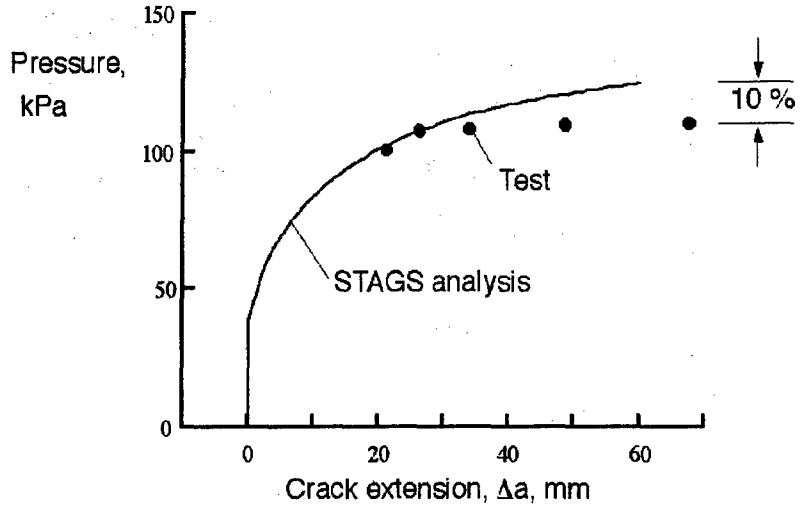

Figure 11. Panel ASIP1 test-analysis correlation of crack extension results as a function of pressure.

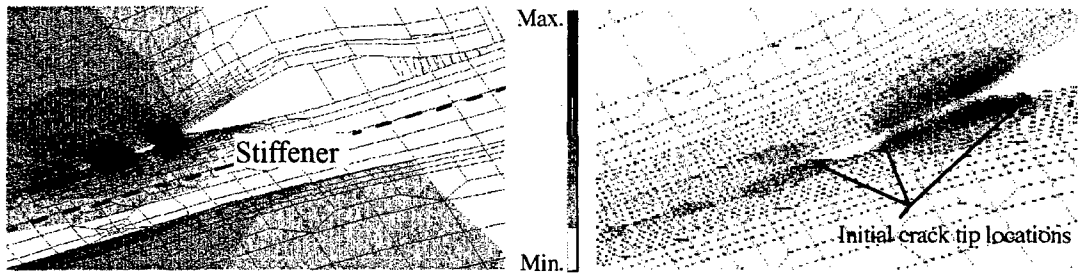

(a) Hoop stress, σ_y (b) Plastic hoop strain, $(\varepsilon_y)_p$

Figure 12. Typical analysis results for panel ASIP2 showing crack growth in the lead crack and MSD cracks.

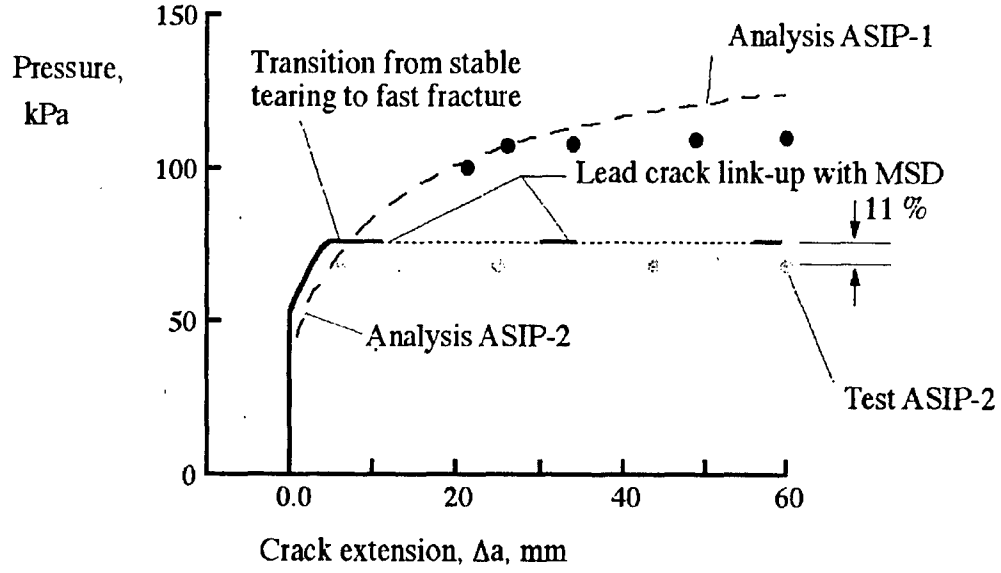

Figure 13. Panel ASIP2 test-analysis correlation of crack extension results as a function of pressure.